Optical set-up for the digital camera system at FNPL

P. Piot[1], Y.-E. Sun[2]
[1] *Fermilab, Batavia, IL 60510, USA*
[2] *University of Chicago*

September 15, 2004

Abstract

We present the foreseen optical set-up for the upgraded beam viewer imaging system at FNPL. The use of digital camera will enhance the performance of optical transition radiation and YaG-based beam viewers. Measurement of the whole system resolution (including camera, optics and digitizer) is also presented.

1 Upgraded Imaging system

At FNPL (Fermilab/NICADD Photoinjector Laboratory) the beam transverse density is measured using intecepting screens to generate either optical transition radition (OTR) or fluorescence (using YaG-laminated screens). The screen normal axis makes a 45° angle with the beam propagation axis and the radiation is emitted centered around the specular axis, i.e. 90° w.r.t. the beam propagation axis. The screen is located in a six-way cross (see Fig. 1) allowing the radiation to be extracted from vacuum via an optical window mounted on one of the six-way cross port. In our configuration, the radiation shines along the horizontal axis. A 45° mirror mounted downstream of the extraction window reflects the radiation toward the floor of the tunnel. The radiation is then collected by an optical system consisting of CCD- SONY camera [1] equipped with a PENTAX 50 mm lens [2] (see Fig. 1). The choice of the SONY camera was dictated by its dynamical range (up to 10 bits) and the size of the pixel array (728× 1024). The CCD is mounted vertically below the beamline axis for better shielding. Analytically we estimated a focal length of 50 mm should provide the proper magnification to demagnify the viewer circular area with axes $22.5 \times 22.5/\sqrt{2}$ mm^2 onto the CCD array of dimension $4.8x3.6$ mm^2 (the array consists of 1024×768 pixels, each pixel being a square of 4.65 μm).

We have optimized the imaging system by adjusting two parameters: (1) the spacing between the PENTAX lens and the CCD array of the camera and (2) the length between the PENTAX lens and the to-be-imaged OTR screen. The approximated optimal distances are reported in Fig. 1, and the corresponding image of the screen is shown in Fig. 2. The pixel size in the object plane are found to be 21 and 23 microns for the horizontal and vertical directions respectively (the 9% difference the calibration for the two axis maybe attributed

to the screen tilt angle not being exactly 45° during our measurements). To achieved the necessary demagnification, a spacer of 9 mm length had to be placed between the lens and the camera C-mount.

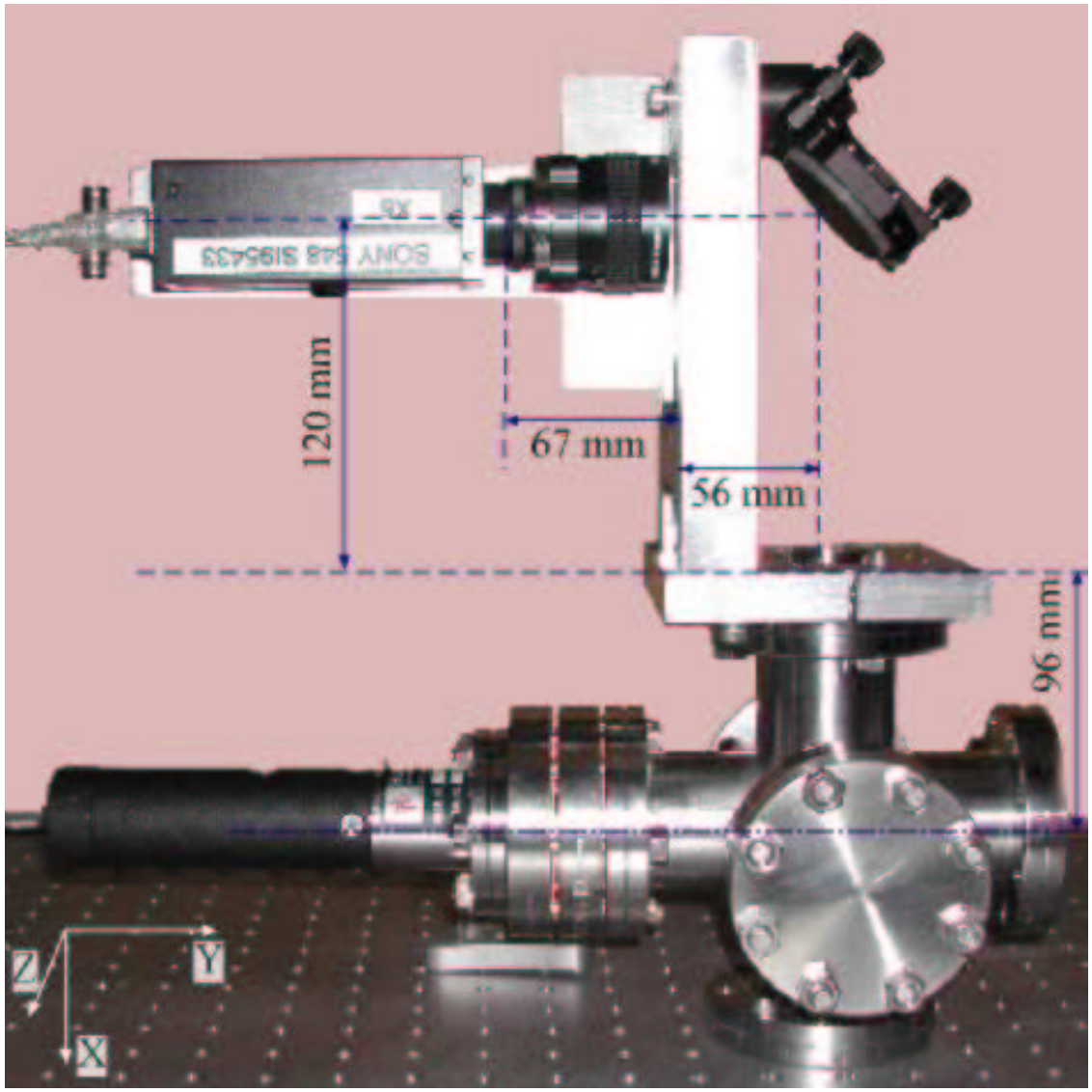

Figure 1: Overview of the optical system with approximate distances between various elements. The beam propagates along the z-axis and is intercepted by an aluminum screen located in the 6-ways cross. The normal axis of the aluminum screen makes a 45° angle with z and the backward OTR light shines out of the top port of the 6-way cross. In the accelerator, the camera is indeed mounted along the vertical direction.

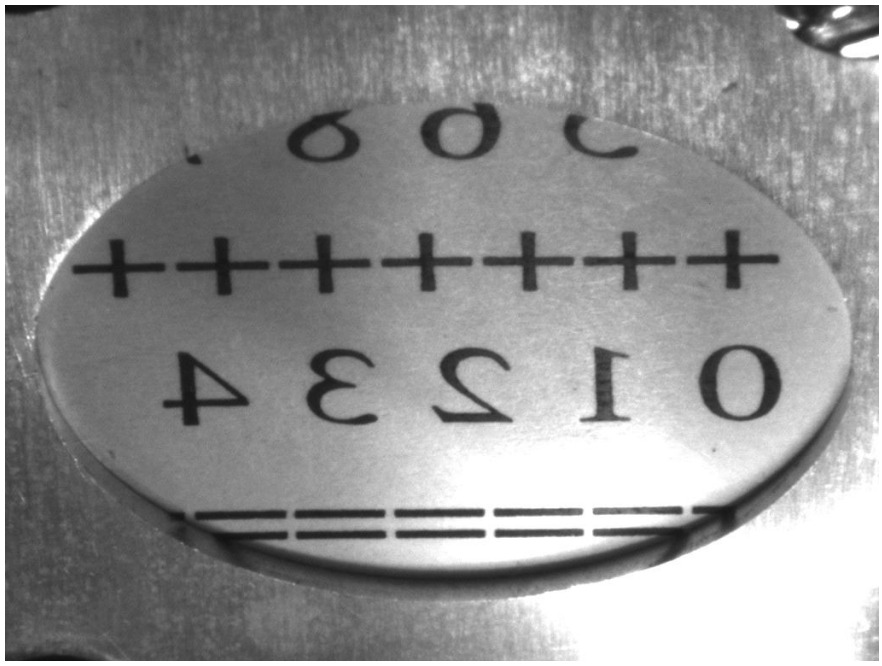

Figure 2: Example of calibration pattern. Horizontal and vertical axis for this picture correspond respectively to y and x directions in the accelerator (see also Fig. 1).

2 Resolution measurements

2.1 Diffraction versus depth-of-field

We assumes the gain, and shutter setting on the digital camera do not significantly influence the resolution of the system (as long as the system is operated in the linear regime). Such an assumption was verified in early test of the SONY CCD camera [3].

Given the optical set-up we devised in the previous Section, the resolution of the system will essentially depends on the manual iris aperture used in the lens system. Although the iris main purpose is to provide a controllable attenuation of the OTR intensity reaching the CCD array, it also affects the resolution via depth-of-field and diffraction effects.

The diffraction effects for a cylindrical symmetric system limited by an aperture of diameter D is quantify by the Raleigh criterion: two point-sources (radiating at wavelength λ) separated by an angle larger than $\delta\theta \simeq 1.22\lambda/D$ can be resolved by the optical system. if L is the distance between the object plane and the aperture, and δx the distance between the two point-sources, we have the diffraction resolution limit $\delta x \simeq 1.22\lambda/\psi$ wherein ψ is the angle subtended by the aperture: $\tan\psi = D/L$. The factor 1.22 in the previous equations come from the fact the resolution is defined in term of the Airy disk radius, i.e. the first zero of the function $J_1(\zeta)/\zeta$ ($1.22 \simeq 3.832/\pi$). In our case we are interested in the root mean square (rms) resolution and we define it by replacing the factor 1.22 by 0.49 ($\simeq 1.553/\pi$) deduced from the calculation of the rms size of the airy disk. We finally estimate the diffraction-limited rms resolution to be about $\sigma_{dif} \simeq 0.49\lambda/\mathrm{atan}(f/(2FL))$ wherein

$F \doteq f/D$ is the F-number of the system (f is the focal length and D the aperture diameter). Taking $\lambda = 440$ nm, $L = 300$ mm, and $f = 50$ mm we found $\sigma \in [0.34, 1.8]$ pixels for $F \in [2.6, 16]$.

The depth-of-field effects is estimated to yield a resolution limit of $\delta x \simeq 4F^2\lambda$. The depth-of-field, contrary to diffraction effect, calls for a small iris diameter.

2.1.1 Measurement technique

In principle the resolution measurement consists in measuring the modulation transfer function of the optical system for various modulation patterns. In practice one uses a special target (so-called USFA 1951 target), which is pictured in Figure 5, to do such a measurement [5]. In the present case although we use such a target, we measured the resolution using the so-called sharp edge technique: we measure the resolution using the sharp edge of the various bars drawn on the target. In signal processing theory, the resolution of a system is defined as a measure of the system response to an input impulsion (δ-like signal). However the generation of a δ-like point light source is no easy in practice. A common technique is to instead use a sharp edge (Heaviside function). If we assume the system to be linear so that the input image signal $I(x, y)$ is mapped to an output image signal $O(x, y)$ via a relation of the form $I(x, y) \to O(x, y) = \sum_\lambda a_\lambda I(x, y)$, then upon differentiation w.r.t., e.g., x, we also have a relation of the form $\partial_x I(x, y) \to \partial_x O(x, y) = \sum_\lambda a_\lambda \partial_x I(x, y)$ (wherein ∂_x refers to the derivative w.r.t. x variable). The latter results means that measuring the response function to an impulsion δ-like input (i.e. $I(x, y) = \delta(x)$)is equivalent to measuring the response of the system to a sharp transition Heaviside-like function (i.e. $I(x, y) = H(x)$) since the former function is the spatial derivative of the latter function.

In practice we used the bars provided by the USAF target, and we assume these bars to be perfect. Let's consider a vertical bars with width $2d$ along the horizontal axis; its normalized intensity distribution can be formulated as:

$$\hat{I}(x, y) = \frac{1}{2}\left(H(x + d) + H(-x + d)\right) \tag{1}$$

wherein H is the Heavide function $H(\zeta) = 1$ for $\zeta > 0$ and $H(\zeta) = 0$ elsewhere). The derivative of $\hat{I}(x, y)$ with respect to x is then

$$\partial_x \hat{I}(x, y) = \frac{1}{2}\left(\delta(x + d) - \delta(x - d)\right) \tag{2}$$

Let's assume the latter signal is injected in a perfect (no resolution limit) optical system, the output signal will be given by $\partial_x \hat{O}(x, y) \propto \partial_x \hat{I}(x, y)$. However the fact the system has a finite resolution means an input δ-function is going to widen. We assume the output function corresponding to an input δ-function to be a Gaussian distribution *, then we can replace Eq. 2:

$$\partial_x \hat{O}(x, y) \propto \left(\exp\left(-\frac{(x + d)^2}{2\sigma_x^2}\right) - \exp\left(-\frac{(x - d)^2}{2\sigma_x^2}\right)\right) \tag{3}$$

*this is motivated by the simple fact that a δ-function can be viewed as a Gaussian function with variance taken to zero.

Then upon integration ($\int_{-\infty}^{x} d\xi \partial_x \hat{O}(\xi, y)$) we obtain:

$$\hat{O}(x, y) = A \left(\mathrm{erf}\left(\frac{x+d}{\sqrt{2}\sigma_x} \right) - \mathrm{erf}\left(\frac{x-d}{\sqrt{2}\sigma_x} \right) \right). \tag{4}$$

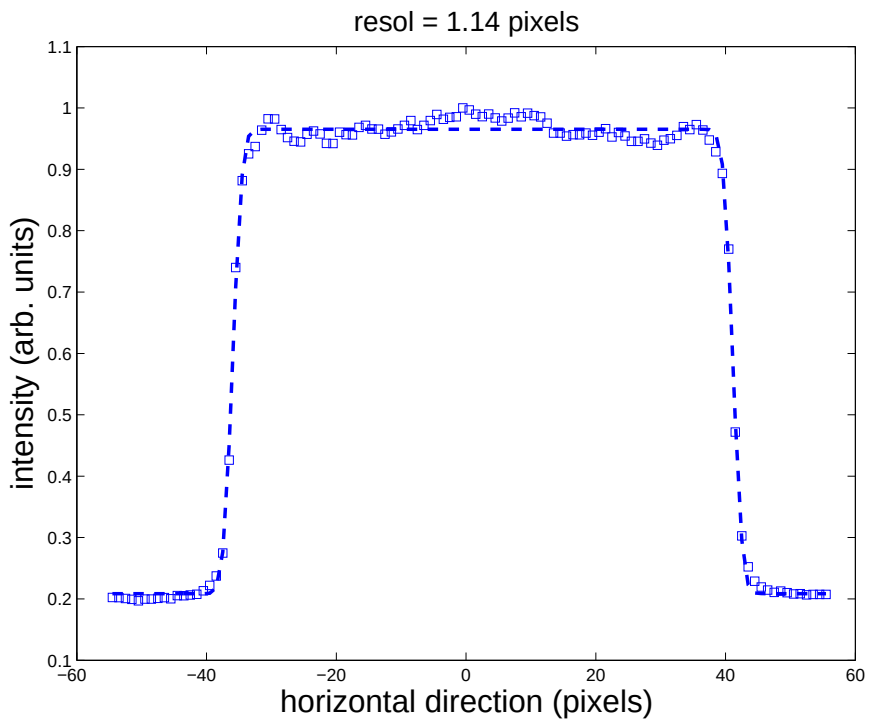

Figure 3: Example of resolution measurement from a fitting of the profile or a rectangular bar of the USAF target (see Fig. 5).

Thus from the USAF target, we can measure profiles associated to bars. This profile can then be fitted with Eq. 4, A, d, and σ_x begin the fit parameters, to yield the resolution (σ_x) of the system. An example of such a fit on a bar profile is presented in Fig. 3.

2.1.2 Experimental set-up and results

The system depicts in Fig. 1 was used to measure the resolution. The camera was first focused on the screen (to yield an image similar to the one presented in Fig. 2). The mirror was then removed and an USAF resolution target was located in front of the camera at a distance similar to the distance to the screen (the distance was adjusted to produced a well focused image of the target). An example of target image is shown in Fig. 5. The target image was back illuminated using white light (we however expect chromatic effect in the optical system to be very small over the visible spectrum since the lens are said to be optimized to reduce chromatic effects [4]).

Using the sharp edge technique afore-described, we measured the resolution of the system for various iris diameters (or F-numbers). The results are shown in Fig. 4. For F-Numbers

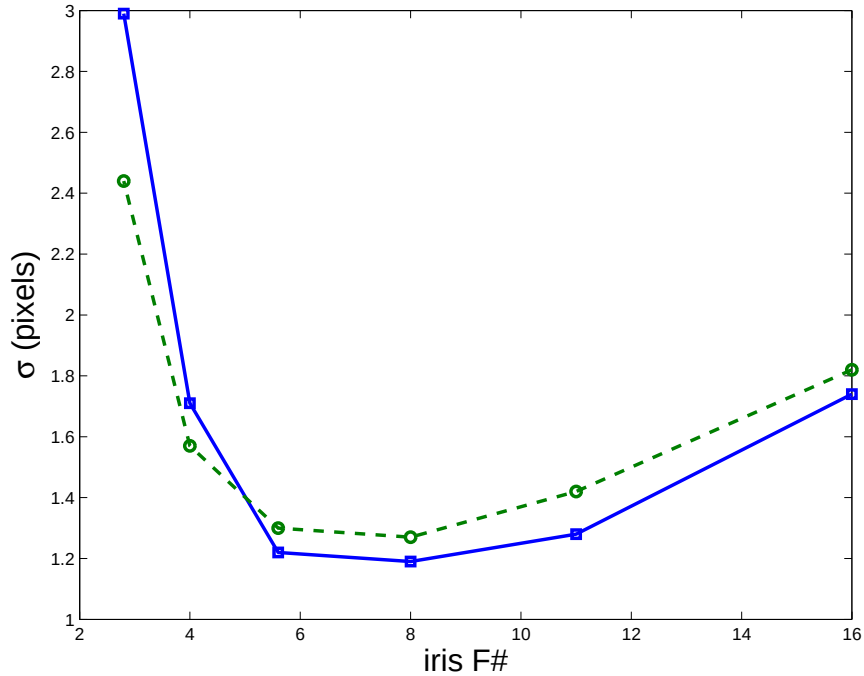

Figure 4: Measured resolution for vertical (squares) and horizontal (circles) directions versus iris F-number.

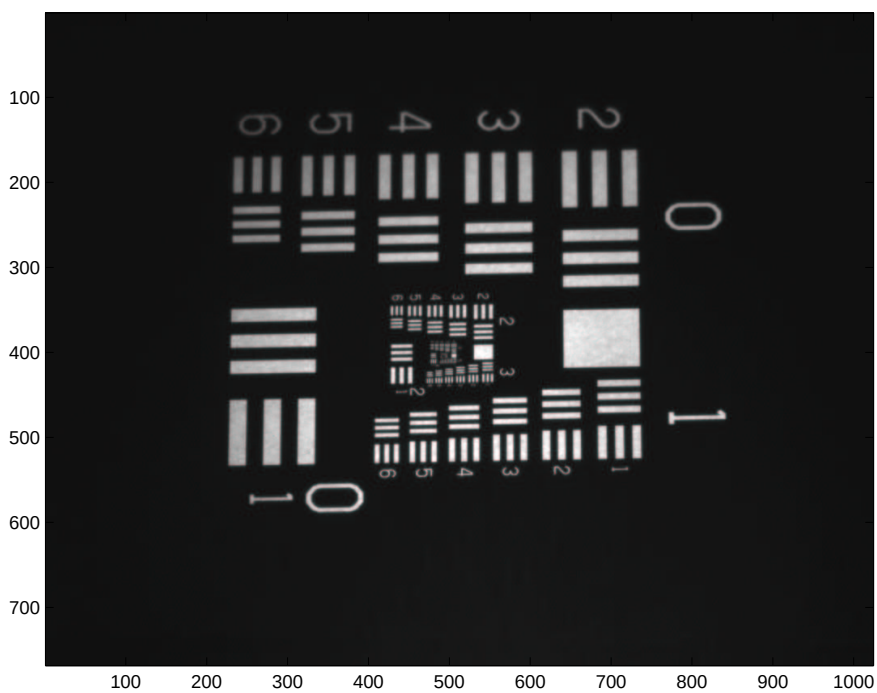

Figure 5: Example of image of the USAF target. For this image, the F-number is $F = 8$.

$F \in [5.6, 11]$, the resolution is about 1.3 times the pixel size in the object plane, that is $23 \times 1.3 \simeq 30$ μm. For larger F-numbers $F \geq 11$ the resolution limit increases due to

diffraction effects, whereas for smaller F-numbers $F \leq 6$, it degrades due to depth-of-field effects.

3 Optical transition radiation intensity

It is finally interesting to estimate the amount of OTR radiation that is captured by the optical system as the F-number of the system is varied. If we estimate the half-angular acceptance of the system to be approximately $\theta \simeq \mathrm{atan}(f/(2FL))$ and assume the system to be centered on the radiation source emission axis, then the fraction radiated intensity within a cone of half-angle θ is (see also [6]):

$$R(\theta) = \frac{\int_0^{\theta} \frac{\sin^3 \vartheta}{(1-\beta^2 \cos^2 \vartheta)^2} d\vartheta}{\int_0^{\pi/2} \frac{\sin^3 \vartheta}{(1-\beta^2 \cos^2 \vartheta)^2} d\vartheta} \tag{5}$$

The latter function is plotted in Fig. 6, where we compare the expected normalized OTR

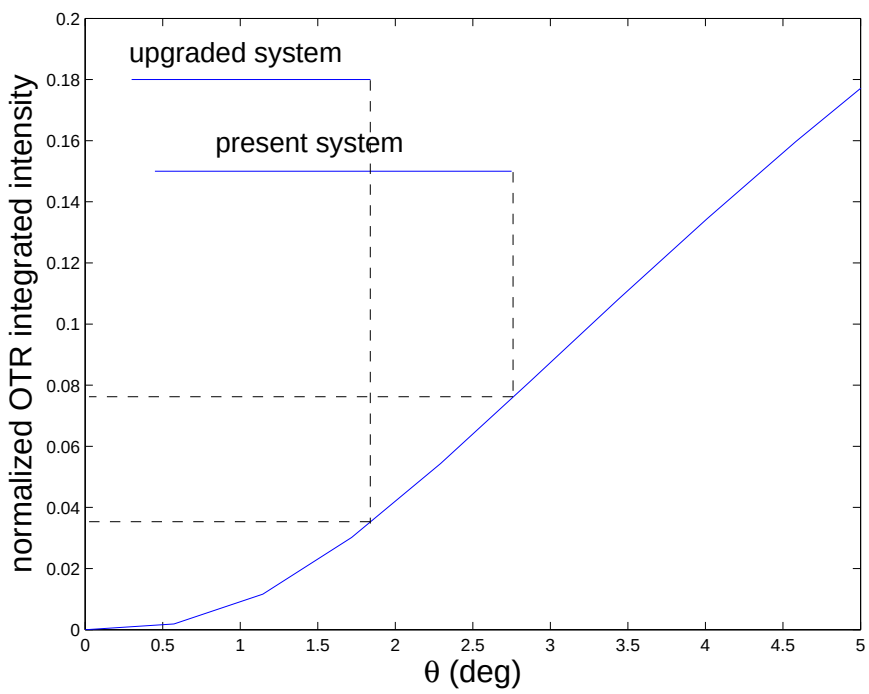

Figure 6: Normalized OTR intensity versus half-angle acceptance of the optical system. The normalization is done w.r.t. the total intensity emitted within a half-angle acceptance of 90°.

intensity for the upgraded system with respect to the present system. Since the lens is located at 300 mm from the screen (compared to 100 mm in the present case), the intensity will drop by a factor of approximately 2. Such a reduction in OTR intensity should not pose any problem for detecting the OTR signal.

References

[1] SONY digital camera model number XCD-X710

[2] model number C-mount C25011 see documentation at
http://www.pentaxusa.com/pdf/Manual_Iris_Lenses_Pages.pdf

[3] J. Wennerberg, unpublished results and private communication July 2004

[4] information from PENTAX USA web-site

[5] see "USFA 1951 and microscopy resolution test charts" available at
http://www.efg2.com/Lab/ImageProcessing/TestTargets

[6] M. Hüning, Beams-doc-652-v1 available at
http://beamdocs.fnal.gov/cgi-bin/public/DocDB/ShowDocument?docid=652&version=1